Nanoscale

COMMUNICATION

View Article Online
View Journal | View Issue

Cite this: *Nanoscale*, 2014, **6**, 10530

Received 14th May 2014
Accepted 8th July 2014

DOI: 10.1039/c4nr02634a

www.rsc.org/nanoscale

Broadband ultrafast nonlinear absorption and nonlinear refraction of layered molybdenum dichalcogenide semiconductors†

Kangpeng Wang,[ab] Yanyan Feng,[a] Chunxia Chang,[a] Jingxin Zhan,[a] Chengwei Wang,[c] Quanzhong Zhao,[c] Jonathan N. Coleman,[b] Long Zhang,*[a] Werner J. Blau[ab] and Jun Wang*[ac]

A series of layered molybdenum dichalcogenides, *i.e.*, MoX_2 (X = S, Se and Te), were prepared in cyclohexyl pyrrolidinone by a liquid-phase exfoliation technique. The high quality of the two-dimensional nanostructures was verified by transmission electron microscopy and absorption spectroscopy. Open- and closed-aperture *Z*-scans were employed to study the nonlinear absorption and nonlinear refraction of the MoX_2 dispersions, respectively. All the three-layered nanostructures exhibit prominent ultrafast saturable absorption (SA) for both femtosecond (fs) and picosecond (ps) laser pulses over a broad wavelength range from the visible to the near infrared. While the dispersions treated with low-speed centrifugation (1500 rpm) have an SA response, and the MoS_2 and $MoSe_2$ dispersions after higher speed centrifugation (10 000 rpm) possess two-photon absorption for fs pulses at 1030 nm, which is due to the significant reduction of the average thickness of the nanosheets; hence, the broadening of band gap. In addition, all dispersions show obvious nonlinear self-defocusing for ps pulses at both 1064 nm and 532 nm, resulting from the thermally-induced nonlinear refractive index. The versatile ultrafast nonlinear properties imply a huge potential of the layered MoX_2 semiconductors in the development of nanophotonic devices, such as mode-lockers, optical limiters, optical switches, *etc.*

Introduction

Owing to the specific two-dimensional (2D) confinement of electron motion and the absence of interlayer perturbation, layered 2D crystals of semiconducting transition metal dichalcogenides (TMDs) are considered as promising materials for emerging applications in nanoelectronic, micromechanic, and nano-optoelectronic devices with high performance and unique functions.[1–5] The TMD materials, such as MoX_2 and WX_2 (X = S, Se, Te) possess similar lattice structures and show layer-dependent properties, *e.g.*, indirect-to-direct band gap transition as the decreasing of the number of monolayer.[1,6–9] Thus far, a series of photonic properties, such as visible photoluminescence, transient absorption, and second and third harmonic generations. have been demonstrated in 2D TMD structures.[10–16] We recently reported for the first time, to the best of our knowledge, the prominent ultrafast saturable absorption (SA) performance in layered MoS_2 nanosheets in the near-infrared (NIR) region.[17] These extraordinary photonic properties open the door to TMD-based nanophotonic devices, such as optical switches, pulse-shaping devices, mode-lockers, optical limiters, *etc.*, capable of ultrafast response and broadband tenability.[17–20]

For the sake of developing high performance photonic devices, it is undoubtedly important to have a comprehensive understanding on the fundamental ultrafast and nonlinear optical (NLO) properties of the working substances. In this work, a series of dispersions containing a large population of pristine molybdenum dichalcogenide nanosheets were dispersed in cyclohexyl pyrrolidinone (CHP) by a high-yield liquid-exfoliation (LPE) technique.[21–23] The absorption spectroscopy and transmission electron microscopy (TEM) characterizations showed the high quality of the layered nanostructures. We systematically study the nonlinear absorption and nonlinear refraction properties of the layered MoX_2 nanostructures by *Z*-scan over a broad temporal (ps–fs) and spectral (Vis-NIR) range.

Results and discussion

The liquid exfoliation has been proven to be a simple, effective and productive technique for exfoliating layered TMD crystals and preparing high-quality 2D nanostructures.[21–23] The stable dispersions of layered TMD materials can be obtained, provided that the surface energy of the solvent matches well with that of

[a]*Key Laboratory of Materials for High-Power Laser, Shanghai Institute of Optics and Fine Mechanics, Chinese Academy of Sciences, Shanghai 201800, China*

[b]*School of Physics and the Centre for Research on Adaptive Nanostructures and Nanodevices (CRANN), Trinity College Dublin, Dublin 2, Ireland*

[c]*State Key Laboratory of High Field Laser Physics, Shanghai Institute of Optics and Fine Mechanics, Chinese Academy of Sciences, Shanghai 201800, China*

† Electronic supplementary information (ESI) available: Electron scattering patterns from TEM characterizations of MX_2 nanosheets; CA *Z*-scan results of graphene dispersions in the ps region. See DOI: 10.1039/c4nr02634a

the layered materials. In this work, CHP was utilized to disperse MoS_2, $MoTe_2$, and $MoSe_2$, respectively. The initial dispersions were treated for 60 min by a high-power sonication tip. After sonication, the dispersions were allowed to settle for ~24 h before centrifuging to remove large sedimentations. The top two-thirds of the dispersions were collected after centrifugation at 1500 rpm for 90 min. All dispersions are stable against sedimentation, and no further aggregation was observed for weeks (see Fig. S1†).

In general, the MoX_2 dispersions prepared by LPE are composed of monolayers and few layers.[21,23] TEM was employed to confirm the status of the dispersed nanosheets. The specimens were prepared by dropping a few milliliters of each dispersion on copper holey carbon grids (mesh size 400). Low-magnification TEM images of typical flakes in the three dispersions are showed in Fig. 1(a)–(c). It appears that most of the nanosheets in the three dispersions are few-layer flakes. At the edge of the nanosheets, very few-layer structures can be seen, as indicated by the dashed boxes in Fig. 1(a)–(c). Fig. 1(d)–(f) show high-magnification images from the nanosheet edges located in the dashed boxes. All the HRTEM images were first processed by fast Fourier transform with a digital periodic filter and then inverse fast Fourier transform to obtain images for lower noise and better clearance of atoms. The fine atomic structures of MoS_2, $MoSe_2$, and $MoTe_2$, together with electron diffraction patterns (see Fig. S2†), imply that the 2H structures of molybdenum dichalcogenides remain undistorted after LPE preparation.[21,23] The pixel intensity distributions along the neighboring atoms are illustrated on the right side of Fig. 1(d)–(f). The number of monolayers in the nanosheets could be roughly deduced by pixel intensity analysis of the neighboring atoms.[21] As for MoS_2 in Fig. 1(d), the neighboring atoms show similar intensity, while for $MoSe_2$ and $MoTe_2$, neighboring atoms appear to be of high contrast in intensity. Therefore, the MoS_2 nanosheet in Fig. 1(d) seems to have even number of monolayers, while $MoSe_2$ and $MoTe_2$ appear very likely to be mono- or triple layered. Nonetheless, the dispersions used in this work were dominated by multilayer nanosheets.

Absorption spectroscopic characterization was carried out for the three MoX_2 dispersions. As shown in Fig. 2, the absorption spectra are comparable with those of previous studies,[22] confirming the existence of high-quality nanosheets in dispersions. It is clearly seen that the characteristic A and B exciton peaks of MoS_2 and $MoSe_2$, originating from the inter-band excitonic transition at the *K* point are located at 673 nm (1.84 eV) and 612 nm (2.03 eV), and 810 nm (1.53 eV) and708 nm (1.75 eV), respectively, indicating a pristine 2H poly-type.[24,25] Referring to the relationship between exciton energy of the A peak and the thickness of the MoS_2 nanosheets, one can estimate the average thickness of the nanosheets in the MoS_2 dispersions to be >8 nm, equivalent to ~15 monolayers.[10]

Open-aperture (OA) and closed-aperture (CA) *Z*-scans were employed to study the nonlinear absorption and nonlinear refraction of the MoX_2 dispersions, respectively.[17,26–28] The OA *Z*-scan measures total transmittance through the sample as a function of incident laser intensity, while the sample is sequentially moved through the focus of a lens (along the *z*-axis). The optical setup was analogous to that used in the previous experiments in measuring the NLO response of the nanomaterials.[17,29,30] For the CA *Z*-scan, an aperture was placed right after the sample dispersions to confine the transmitted beam incident on the detector. With the help of the *Z*-scan, the dispersions were characterized using the laser sources with different wavelength and pulse-duration parameters, *i.e.*, 1 kHz, 100 fs pulses at 800 nm from a Ti: sapphire mode-lock laser, 0.1 kHz, 340 fs pulses at 1030 nm and its second harmonic, 515 nm, from a chirped pulse-amplified fiber laser, and 10 kHz, 100 ps pulses at 1064 nm and 532 nm from a ps fiber laser. During the measurements, unwanted NLO effects, such as super-continuum generation from the solvent CHP and nonlinear scattering have been carefully avoided using low-intensity pulses and employing pure CHP for reference testing. Fig. 3 and 4 show the typical *Z*-scan results for fs and ps lasers, respectively.

As shown in Fig. 3(a) and (c) and 4(a) and (b), all three molybdenum dichalcogenides, MoS_2, $MoSe_2$ and $MoTe_2$, exhibit obvious saturable absorption response from the visible (515 and 532 nm) to NIR (800, 1030 and 1064 nm) regions for both fs and ps pulses with various repetition rates (0.1, 1, and 10 kHz), implying a broadband ultrafast NLO performance. The molybdenum dichalcogenides are well known for the unique band

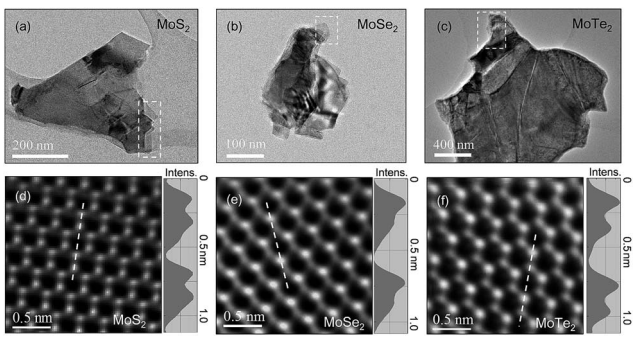

Fig. 1 TEM images of layered MoS_2, $MoSe_2$, $MoTe_2$ nanoflakes. (a)–(c) Overviews of the nanoflakes. (d) and (e) High-magnification TEM images of the few-layer nanosheets. Right side graphs show the intensity distribution along the dashed lines.

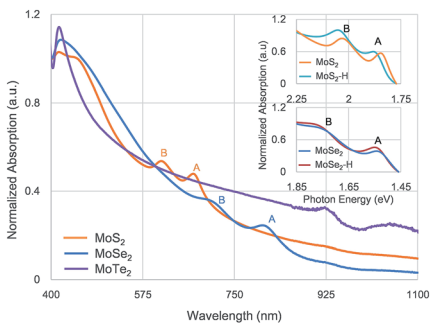

Fig. 2 Absorption spectra of the MoX_2 dispersions. Insets: shift of the A and B exciton peaks for the MoS_2 and $MoSe_2$ dispersions with a low-speed centrifugation treatment (MoX_2) and higher speed treatment (MoX_2–H).

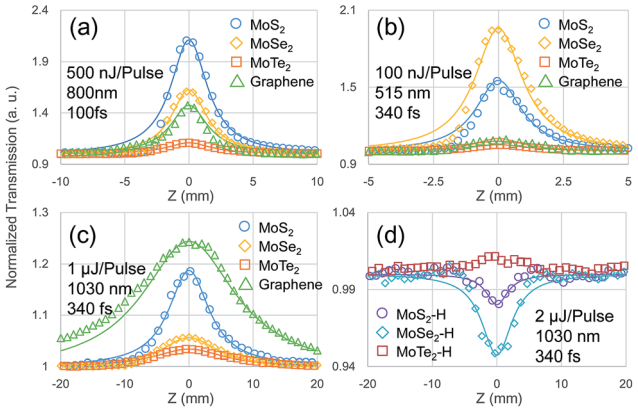

Fig. 3 OA Z-scan results of the MoX_2 dispersions in the fs region. Samples in (a)–(c) exhibit obvious SA response, while showing TPA response in (d) for the MoS_2 and $MoSe_2$ dispersions with a higher speed centrifugation treatment (10 000 rpm).

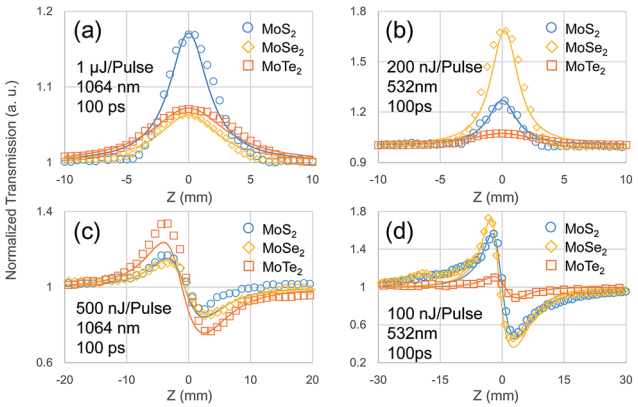

Fig. 4 Z-scan results of the MoX_2 dispersions for the ps pulses. (a) and (b) OA Z-scan results at 1064 nm and 532 nm. (c) and (d) CA Z-scan results. All of the dispersions exhibit self-defocusing shapes.

gap transition from indirect to direct when the layered structure reduces from bulk to monolayer. The indirect band gaps for the multilayer MoS_2, $MoSe_2$ and $MoTe_2$ were determined to be 1.2 eV (1033 nm), 1.1 eV (1128 nm) and 1.0 eV (1239 nm), respectively. In contrast, the direct band gaps for the monolayer MoX_2 are increased to 1.8 eV (690 nm), 1.5 eV (828 nm) and 1.1 eV (1128 nm), respectively.[1] In general, semiconductors with band gaps smaller than the incident photon energy exhibit saturable absorption, resulting from the free-carrier excitation from valence band to conduction band and hence Pauli-blocking. However, photons with energy less than the band gap will not be able to excite electrons/holes directly to the conduction/valence bands unless two photons are simultaneously absorbed, *i.e.*, two-photon absorption (TPA) takes place. In contrast to SA, TPA results in the normalized transmission decrease when the incident intensity increases, leading to a valley centered at the focal point in the Z-scan curve.

Laser pulses at 515 and 532 nm can induce SA for the MoS_2 monolayer with a band gap of ~1.8 eV (~690 nm), while pulses at 800, 1030, and 1064 nm are able to generate TPA. In contrast, the few-layer MoS_2 with a band gap of ~1.2 eV (~1033 nm) exhibit SA for all wavelengths used in this work. SA responses in Fig. 3(a)–(c) and 4(a) and (b) are attributed to the domination of few-layer nanosheets in the dispersions. TPA from the minority monolayers would be screened by the strong SA in the majority fewlayer nanosheets as we predicted in a previous study.[31] Similarly, by comparing the band gaps of few-layer $MoSe_2$ and $MoTe_2$ with the incident photon energies, it is confirmed that the $MoSe_2$ and $MoTe_2$ dispersions possess SA in all of the laser pulses. Although photon energy for pulses at 1064 nm is slightly less than the theoretical prediction of band gap for the few-layer MoS_2, absorption saturation was still observed in the MoS_2 dispersions, which was also reported by other groups.[18,19] The possible reason may be that there is a small difference between the theoretical and practical band gaps or in defect-induced interband states.

Nonlinear absorption coefficient α_{NL} can be deduced by numerically fitting the Z-scan curves with the nonlinear propagation equation $\frac{dI}{dz} = -(\alpha_0 + \alpha_{NL}I)I$, in combination of the Gaussian field approximation after the laser beam was focused by the convex lens.[26,27] The imaginary part of the third-order NLO susceptibility, Im $\chi^{(3)}$, is directly related to α_{NL} by Im $\chi^{(3)} = \left[\frac{10^{-7}c\lambda n^2}{96\pi^2}\right]\alpha_{NL}$, where c, λ, and n are the light speed in vacuum, wavelength of the laser pulses, and the refractive index, respectively. In order to eliminate the discrepancy caused by the linear absorption α_0, we define a figure of merit (FOM) for the third-order optical nonlinearity as FOM $= |\text{Im } \chi^{(3)}/\alpha_0|$. To obtain the saturable intensity I_s, one can use the propagation equation in the form of $\frac{dI}{dz} = -\frac{\alpha_0 I}{1 + I/I_s}$. All linear and NLO parameters deduced from Fig. 3(a)–(c) and 4(a) and (b) are summarized in Table 1. Because the α_0 of each dispersion used in the experiment is different, we mainly adopt FOM as a criterion to evaluate the SA performance of the materials. The use of FOM also helps us to compare with the other nanomaterials reported.[32–35]

Referring to FOM for fs pulses in Table 1, overall, the MoX_2 nanosheets exhibit more pronounced SA response than graphene. At 1030 nm, FOMs for all the three MoX_2 have the same magnitude of 10^{-15} esu cm. FOMs of MoS_2 and $MoTe_2$ are larger than those of $MoSe_2$ and graphene by one order of magnitude at 800 nm, and the comparison between MoS_2 and graphene is consistent with previous results.[31] At the aforementioned two wavelengths, $MoTe_2$ shows the largest FOM among the four dispersions. At 515 nm, FOMs of all the three MoX_2 dispersions exceed those of graphene by one order of magnitude, and $MoSe_2$ turns out to be the material possessing the largest FOM. It should be mentioned that we have found similar regularity by analyzing the saturation intensity I_s presented in Table 1. Graphene dispersions exhibit the largest I_s in comparison with all the MoX_2 dispersions. $MoTe_2$ dispersions show the lowest I_s at both 800 and 1030 nm, whereas the I_s of $MoSe_2$ is the minimum at 515 nm. It is noticed that FOM of the MoX_2 in the ps regime is greater than that in fs by two orders of magnitude. For instance, FOM of MoS_2 for 340 fs pulses at 1030 nm is ~10^{-15} esu cm,

Table 1 Linear and NLO parameters of the three molybdenum dichalcogenide dispersions measured by OA *Z*-scan

Laser	Sample	T (%)	α_0 (cm^{-1})	NLO response	α_{NL} (cm GW^{-1})	Im $\chi^{(3)}$ (esu)	FOM (esu cm)	I_s (GW cm^{-2})
1030 nm, 1 kHz, 340 fs	MoS_2	30.9	11.75	SA	$-(9.17 \pm 2.56) \times 10^{-2}$	$-(6.7 \pm 1.9) \times 10^{-14}$	$(5.7 \pm 1.6) \times 10^{-15}$	114 ± 63
	$MoSe_2$	80.9	2.11	SA	$-(1.29 \pm 0.13) \times 10^{-2}$	$-(9.4 \pm 1.0) \times 10^{-15}$	$(4.22 \pm 0.27) \times 10^{-15}$	121 ± 22
	$MoTe_2$	90.6	0.87	SA	$-(7.50 \pm 0.47) \times 10^{-3}$	$-(5.50 \pm 0.34) \times 10^{-15}$	$(6.38 \pm 0.39) \times 10^{-15}$	68 ± 8
	Graphene	18.1	17.10	SA	$-(9.40 \pm 3.18) \times 10^{-2}$	$-(6.9 \pm 2.3) \times 10^{-14}$	$(4.03 \pm 1.36) \times 10^{-15}$	170 ± 51
800 nm, 1 kHz, 100 fs	MoS_2	32.6	11.22	SA	$-(2.42 \pm 0.80) \times 10^{-2}$	$-(1.38 \pm 0.45) \times 10^{-14}$	$(1.23 \pm 0.40) \times 10^{-15}$	381 ± 346
	$MoSe_2$	45.3	7.93	SA	$-(2.54 \pm 0.60) \times 10^{-3}$	$-(1.45 \pm 0.34) \times 10^{-15}$	$(6.9 \pm 1.6) \times 10^{-16}$	590 ± 225
	$MoTe_2$	86.3	1.47	SA	$-(3.7 \pm 1.2) \times 10^{-3}$	$-(2.13 \pm 0.66) \times 10^{-15}$	$(1.45 \pm 0.45) \times 10^{-15}$	217 ± 11
	Graphene	16.8	17.85	SA	$-(1.52 \pm 0.42) \times 10^{-2}$	$-(8.7 \pm 2.4) \times 10^{-15}$	$(4.9 \pm 1.4) \times 10^{-16}$	583 ± 127
515 nm, 1 kHz, 340 fs	MoS_2	7.94	25.34	SA	$-(0.357 \pm 0.064)$	$-(1.31 \pm 0.23) \times 10^{-13}$	$(5.16 \pm 0.92) \times 10^{-15}$	58 ± 21
	$MoSe_2$	19.38	16.41	SA	$-(0.245 \pm 0.028)$	$-(9.0 \pm 1.0) \times 10^{-14}$	$(5.46 \pm 0.62) \times 10^{-15}$	43 ± 2
	$MoTe_2$	87.60	1.32	SA	$-(1.42 \pm 0.03) \times 10^{-2}$	$-(5.20 \pm 0.12) \times 10^{-15}$	$(3.93 \pm 0.09) \times 10^{-15}$	58 ± 11
	Graphene	13.61	19.94	SA	$-(4.8 \pm 1.3) \times 10^{-2}$	$-(1.75 \pm 0.47) \times 10^{-14}$	$(8.8 \pm 2.3) \times 10^{-16}$	473 ± 219
1064 nm, 10 kHz, 100 ps	MoS_2	31.30	11.62	SA	$-(5.5 \pm 1.3)$	$-(4.18 \pm 0.98) \times 10^{-12}$	$(3.60 \pm 0.84) \times 10^{-13}$	2.1 ± 0.8
	$MoSe_2$	83.01	1.86	SA	$-(2.05 \pm 0.17)$	$-(1.55 \pm 0.13) \times 10^{-12}$	$(8.33 \pm 0.69) \times 10^{-12}$	0.71 ± 0.07
	$MoTe_2$	89.88	1.07	SA	$-(2.99 \pm 0.52)$	$-(2.27 \pm 0.39) \times 10^{-12}$	$(2.12 \pm 0.38) \times 10^{-12}$	0.19 ± 0.04
532 nm, 10 kHz, 100 ps	MoS_2	7.65	25.70	SA	$-(26.2 \pm 8.8)$	$-(9.9 \pm 3.3) \times 10^{-12}$	$(3.9 \pm 1.3) \times 10^{-13}$	1.13 ± 0.52
	$MoSe_2$	21.12	15.55	SA	$-(35.6 \pm 8.0)$	$-(1.35 \pm 0.30) \times 10^{-11}$	$(8.7 \pm 2.0) \times 10^{-13}$	0.39 ± 0.16
	$MoTe_2$	85.14	1.61	SA	$-(5.54 \pm 0.72)$	$-(2.10 \pm 0.27) \times 10^{-12}$	$(1.30 \pm 0.17) \times 10^{-12}$	0.23 ± 0.03
1030 nm, 1 kHz, 340 fs	MoS_2–H	96.61	0.03446	TPA	$(8.0 \pm 1.4) \times 10^{-5}$	$(5.8 \pm 1.0) \times 10^{-17}$	$(1.69 \pm 0.30) \times 10^{-15}$	N/A
	$MoSe_2$–H	96.33	0.03744	TPA	$(2.00 \pm 0.37) \times 10^{-4}$	$(1.47 \pm 0.27) \times 10^{-16}$	$(3.93 \pm 0.72) \times 10^{-15}$	N/A
	$MoTe_2$–H	99.95	0.00050	N/A	N/A	N/A	N/A	N/A

which becomes $\sim 10^{-13}$ esu cm for 100 ps pulses at 1064 nm. $MoSe_2$ and $MoTe_2$ nanosheets in dispersions exhibit the largest FOM at 1064 nm and 532 nm, respectively. Overall, the LPE-prepared MoX_2 dispersions are shown to be promising broadband ultrafast SA materials. Due to the relatively narrow band gap of ~1.0 eV, the few-layer $MoTe_2$ nanosheets show the best SA performance, *i.e.*, the largest FOM and the lowest I_s at NIR, implying a potential as a passive mode-locker working for up to ~1239 nm.

To investigate the dependence of the nonlinear response on the nanosheet size, and hence, bandgap, we prepared another batch of MoX_2 dispersions, which is termed as 'MoX_2–H' (*i.e.*, MoS_2–H, $MoSe_2$–H and $MoTe_2$–H). The MoX_2–H samples were dispersed by CHP as well, with the same procedure as the previous, except that the centrifugation speed was increased to 10 000 rpm. As illustrated in the insets of Fig. 2, A and B exciton peaks of the MoS_2–H and $MoSe_2$–H dispersions show a clear blue shift. The A exciton peak moves to 663 nm (~1.87 eV) and 806 nm (~1.54 eV) for MoS_2–H and $MoSe_2$–H, respectively. From the A exciton position, one can deduce an average thickness of the MoS_2–H nanosheets to be ~4 nm (equivalent to ~6 monolayers),[10] which is much less than that in the MoS_2 dispersions with 1500 rpm (>8 nm). Because there is a distribution for nanosheets with different thicknesses in the LPE-prepared dispersions,[21,23] the smaller average thickness implies a higher percentage of mono- and few-layers out of all nanosheets in a dispersion. It is likely that the H-series dispersions contain a higher percentage of MoX_2 nanosheets with thinner layers compared with the dispersions after the lower speed centrifugation treatment.

The OA *Z*-scan was conducted for the MoX_2–H dispersions under the 1030 nm, 340 fs laser pulses irradiation, and the results are illustrated in Fig. 3(d). Due to the low nanosheet concentration in MoX_2–H dispersions, the 10 mm long pathlength cuvettes were employed to enhance the NLO signal. In contrast to the SA response for the MoX_2 dispersions, *Z*-scan curves for the MoS_2–H and $MoSe_2$–H dispersions exhibit a valley around the focal point. The valley-like response is attributed to TPA of the very-few-layer MoX_2 nanosheets. The band gaps of the very-few-layer MoS_2 and $MoSe_2$ are much larger than the photon energy of laser pulses at 1030 nm (~1.2 eV). The high percentage of the very-few-layer nanosheets in the MoX_2–H dispersions results in the domination of the TPA process over SA. In the experiment, we did not observe any NLO response from the $MoTe_2$–H dispersions, which is probably due to its low content of nanosheets, for example, nearly 100% linear-optical transmittance (see Table 1). Im $\chi^{(3)}$ of MoS_2–H and $MoSe_2$–H are determined to be $(5.84 \pm 1.04) \times 10^{-17}$ and $(1.47 \pm 0.27) \times 10^{-16}$ esu, respectively.

A *Z*-scan was performed to measure the nonlinear refractive index of the three MoX_2 dispersions with the ps and fs laser sources. Using the ps pulses, we observed an obvious nonlinear self-defocusing signal from all dispersions including graphene. The CA *Z*-scan results for the MoX_2 dispersions at 532 and 1064 nm are shown in Fig. 4(c) and (d). The results for graphene dispersions are given in Fig. S3.† For the fs pulses, there is no measurable CA signal from all the samples. An intensity-dependent NLO refractive index can be described by $n = n_0 + n_2 I$, where n_0 is the refractive index of the medium and n_2 is the NLO refractive index, which can be estimated by fitting the CA *Z*-scan results using the model mentioned in literature.[36] The real part of third-order NLO susceptibility Re $\chi^{(3)}$ and n_2 have the relation of Re $\chi^{(3)}(\text{esu}) = \frac{{n_0}^2 c}{12\pi^2} n_2$ cm^2 W^{-1}. Based on the equations, we calculated n_2 and Re $\chi^{(3)}$ parameters given in

Table 2 NLO refractive parameters of the MoX_2 dispersions in the ps region

Laser	Sample	α_0 (cm^{-1})	n_2 ($cm^2\ W^{-1}$) $\times 10^{-12}$	Re $\chi^{(3)}$ (esu) $\times 10^{-11}$
1064 nm, 10 kHz, 100 ps	MoS_2	11.62	$-(0.207 \pm 0.021)$	$-(1.18 \pm 0.12)$
	$MoSe_2$	1.86	$-(0.120 \pm 0.003)$	$-(0.682 \pm 0.018)$
	$MoTe_2$	1.07	$-(0.160 \pm 0.027)$	$-(0.92 \pm 0.15)$
	Graphene	19.46	−13.7	−78.2
532 nm, 10 kHz, 100 ps	MoS_2	25.70	$-(2.5 \pm 1.2)$	$-(14.1 \pm 6.5)$
	$MoSe_2$	15.55	$-(1.82 \pm 0.73)$	$-(10.3 \pm 4.2)$
	$MoTe_2$	1.61	$-(0.11 \pm 0.04)$	$-(0.62 \pm 0.21)$
	Graphene	19.45	−2.34	−13.3

Table 2. Because the thermally-induced nonlinear refractive index change cannot be neglected if the pulse duration is larger than ~30 ps and no CA signal observed in fs region, it is likely that the self-defocusing results from the thermally-induced NLO index.[37] The MoX_2 nanosheets absorb laser energy and then transform it to heat, resulting in thermal expansion and refractive index change of the entire dispersion. In contrast to the longer ps pulses, the fs pulses have much lower average power to deposit, leading to weak, unmeasurable thermally-induced NLO effects. It should be mentioned that we did not observe any significant CA signal from CHP except for the ps pulses at 1064 nm. However, the NLO effect of CHP was still much less than that of the MX_2 dispersions. Re $\chi^{(3)}$ of CHP was determined to be $-(1.07 \pm 0.08) \times 10^{-12}$ esu at 1064 nm.

Conclusions

The NLO responses of the MoS_2, $MoSe_2$, and $MoTe_2$ dispersions prepared by LPE in CHP have been extensively investigated by employing *Z*-scan technique for fs and ps pulses from the visible to NIR. All three MoX_2 dispersions dominated by few-layer nanosheets show evident broadband SA response, and their FOMs exceeds that of graphene in the fs region at 515, 800, and 1030 nm. The nonlinear responses in the ps region seem to be much stronger than those in the fs region. In addition, the dispersions of MoS_2 and $MoSe_2$ prepared by higher speed centrifugation exhibit TPA for fs pulses at 1030 nm. The versatile ultrafast NLO properties of the layered MoX_2 imply a huge potential in the development of nanophotonic devices, including mode-lockers, optical limiters, and optical switches.

Acknowledgements

This work is supported in part by the National Natural Science Foundation of China (no. 61178007, no. 61308034), Science and Technology Commission of Shanghai Municipality (no. 12ZR1451800, Nano Project no. 11nm0502400, Shanghai Pujiang Program 12PJ1409400, and the Excellent Academic Leader of Shanghai no. 10XD1404600). J.N.C. is supported by the ERC Grant SEMANTICS. W.J.B. is supported in part by Science Foundation Ireland (no. 12/IA/1306). J.W. thanks the External Cooperation Program of BIC (Chinese Academy of Sciences, No. 181231KYSB20130007), the National 10000-Talent Program and CAS 100-Talent Program for financial support.

Notes and references

1 Q. H. Wang, K. Kalantar-Zadeh, A. Kis, J. N. Coleman and M. S. Strano, *Nat. Nanotechnol.*, 2012, **7**, 699–712.
2 R. Mas-Balleste, C. Gomez-Navarro, J. Gomez-Herrero and F. Zamora, *Nanoscale*, 2011, **3**, 20–30.
3 S. Z. Butler, S. M. Hollen, L. Cao, Y. Cui, J. A. Gupta, H. R. Gutierrez, T. F. Heinz, S. S. Hong, J. Huang and A. F. Ismach, *ACS Nano*, 2013, **7**, 2898–2926.
4 D. Jariwala, V. K. Sangwan, L. J. Lauhon, T. J. Marks and M. C. Hersam, *ACS Nano*, 2014, **8**, 1102–1110.
5 J.-W. Jiang, H. Park and T. Rabczuk, *Nanoscale*, 2014, **6**, 3618–3625.
6 W. Jin, P.-C. Yeh, N. Zaki, D. Zhang, J. T. Sadowski, A. Al-Mahboob, A. M. van der Zande, D. A. Chenet, J. I. Dadap and I. P. Herman, *Phys. Rev. Lett.*, 2013, **111**, 106801.
7 K. F. Mak, C. Lee, J. Hone, J. Shan and T. F. Heinz, *Phys. Rev. Lett.*, 2010, **105**, 136805.
8 W. Zhao, Z. Ghorannevis, L. Chu, M. Toh, C. Kloc, P.-H. Tan and G. Eda, *ACS Nano*, 2012, **7**, 791–797.
9 Y. Zhang, T.-R. Chang, B. Zhou, Y.-T. Cui, H. Yan, Z. Liu, F. Schmitt, J. Lee, R. Moore and Y. Chen, *Nat. Nanotechnol.*, 2014, **9**, 111.
10 G. Eda, H. Yamaguchi, D. Voiry, T. Fujita, M. Chen and M. Chhowalla, *Nano Lett.*, 2011, **11**, 5111–5116.
11 V. Štengl and J. Henych, *Nanoscale*, 2013, **5**, 3387–3394.
12 H. Shi, R. Yan, S. Bertolazzi, J. Brivio, B. Gao, A. Kis, D. Jena, H. G. Xing and L. Huang, *ACS Nano*, 2013, **7**, 1072–1080.
13 N. Kumar, Q. Cui, F. Ceballos, D. He, Y. Wang and H. Zhao, *Nanoscale*, 2014, **6**, 4915–4919.
14 A. Splendiani, L. Sun, Y. Zhang, T. Li, J. Kim, C.-Y. Chim, G. Galli and F. Wang, *Nano Lett.*, 2010, **10**, 1271–1275.
15 R. Wang, H.-C. Chien, J. Kumar, N. Kumar, H.-Y. Chiu and H. Zhao, *ACS Appl. Mater. Interfaces*, 2014, **6**, 314–318.
16 N. Kumar, S. Najmaei, Q. Cui, F. Ceballos, P. M. Ajayan, J. Lou and H. Zhao, *Phys. Rev. B: Condens. Matter Mater. Phys.*, 2013, **87**, 161403.
17 K. Wang, J. Wang, J. Fan, M. Lotya, A. O'Neill, D. Fox, Y. Feng, X. Zhang, B. Jiang and Q. Zhao, *ACS Nano*, 2013, **7**, 9260–9267.
18 H. Zhang, S. Lu, J. Zheng, J. Du, S. Wen, D. Tang and K. Loh, *Opt. Express*, 2014, **22**, 7249–7260.
19 S. Wang, H. Yu, H. Zhang, A. Wang, M. Zhao, Y. Chen, L. Mei and J. Wang, *Adv. Mater.*, 2014, **26**, 3538–3544.

20 D.-S. Tsai, K.-K. Liu, D.-H. Lien, M.-L. Tsai, C.-F. Kang, C.-A. Lin, L.-J. Li and J.-H. He, *ACS Nano*, 2013, **7**, 3905–3911.
21 J. N. Coleman, M. Lotya, A. O'Neill, S. D. Bergin, P. J. King, U. Khan, K. Young, A. Gaucher, S. De and R. J. Smith, *Science*, 2011, **331**, 568–571.
22 G. Cunningham, M. Lotya, C. S. Cucinotta, S. Sanvito, S. D. Bergin, R. Menzel, M. S. Shaffer and J. N. Coleman, *ACS Nano*, 2012, **6**, 3468–3480.
23 V. Nicolosi, M. Chhowalla, M. G. Kanatzidis, M. S. Strano and J. N. Coleman, *Science*, 2013, 340.
24 R. Bromley, R. Murray and A. Yoffe, *J. Phys. C: Solid State Phys.*, 1972, **5**, 759.
25 A. Beal, J. Knights and W. Liang, *J. Phys. C: Solid State Phys.*, 1972, **5**, 3540.
26 M. Sheik-Bahae, A. A. Said, T.-H. Wei, D. J. Hagan and E. W. Van Stryland, *IEEE J. Quantum Electron.*, 1990, **26**, 760–769.
27 M. Sheik-Bahae, A. A. Said and E. W. Van Stryland, *Opt. Lett.*, 1989, **14**, 955–957.
28 H. Yan and J. Wei, *Photonics Research*, 2014, **2**, 51–58.
29 J. Wang, Y. Hernandez, M. Lotya, J. N. Coleman and W. J. Blau, *Adv. Mater.*, 2009, **21**, 2430–2435.
30 J. Li, H. Guo and Z.-y. Li, *Photonics Research*, 2013, **1**, 28–41.
31 K. Wang, J. Wang, J. Fan, M. Lotya, A. O'Neill, D. Fox, Y. Feng, X. Zhang, B. Jiang, Q. Zhao, H. Zhang, J. N. Coleman, L. Zhang and W. J. Blau, *ACS Nano*, 2013, **7**, 9260–9267.
32 S. Kumar, M. Anija, N. Kamaraju, K. Vasu, K. Subrahmanyam, A. Sood and C. Rao, *Appl. Phys. Lett.*, 2009, **95**, 191911.
33 S. Kumar, N. Kamaraju, K. Vasu, A. Nag, A. Sood and C. Rao, *Chem. Phys. Lett.*, 2010, **499**, 152–157.
34 H. I. Elim, W. Ji, M.-T. Ng and J. J. Vittal, *Appl. Phys. Lett.*, 2007, **90**, 033106.
35 H. I. Elim, J. Yang, J.-Y. Lee, J. Mi and W. Ji, *Appl. Phys. Lett.*, 2006, **88**, 083107.
36 C. H. Kwak, Y. L. Lee and S. G. Kim, *J. Opt. Soc. Am. B*, 1999, **16**, 600–604.
37 R. W. Boyd, *Science*, Elsevier, 3rd edn, 2010, ch. 4, p. 240.